

Limbal Stem Cells on Bacterial Nanocellulose Carriers for Ocular Surface Regeneration

MSc I. Anton-Sales ¹, Dr L. Koivusalo ², Prof H. Skottman ^{*2}, Dr A. Laromaine ^{*1} and Prof A. Roig ^{*1}

¹ Institute of Materials Science of Barcelona (ICMAB-CSIC), Campus UAB, Bellaterra, Spain. Contact:

alaromaine@icmab.es , roig@icmab.es

² Faculty of Medicine and Health Technology, Tampere University, Arvo Ylpön katu 34, 33520

Tampere, Finland. Contact: heli.skottman@tuni.fi

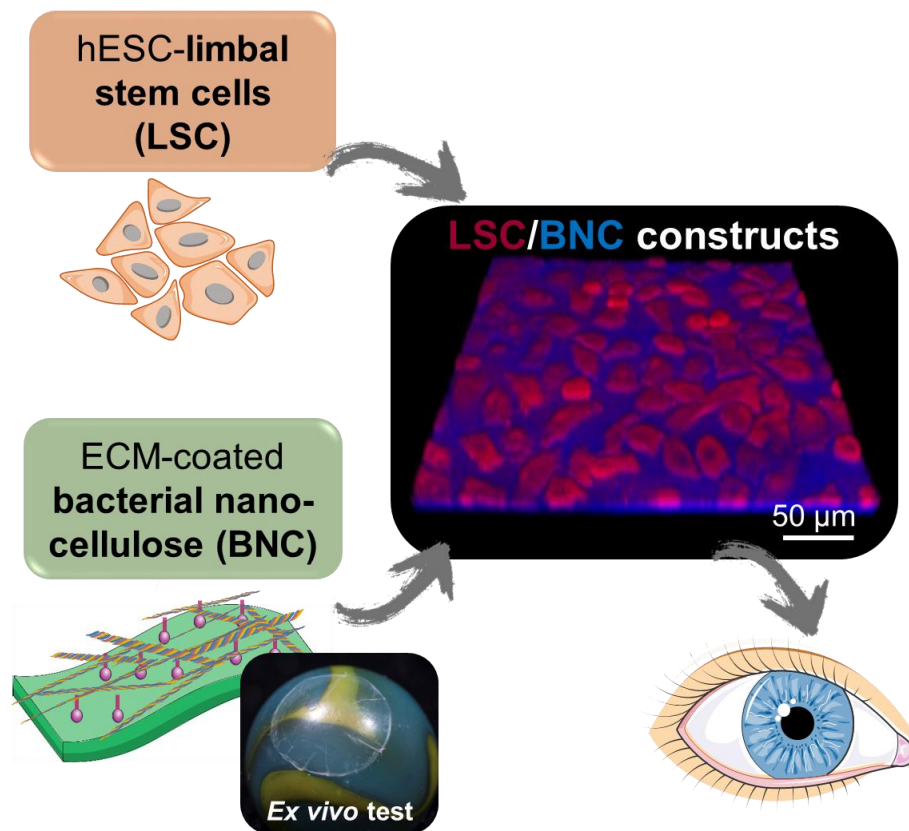
1. ABSTRACT

Limbal stem cells (LSC) are already used in cell-based treatments for ocular surface disorders. Clinical translation of LSCs-based therapies critically depends on the successful delivery, survival and retention of these therapeutic cells to the desired region. Such a major bottleneck could be overcome by using an appropriate carrier to provide anchoring sites and structural support to LSC culture and transplantation. Bacterial nanocellulose (BNC) is an appealing, yet unexplored, candidate for this application because of its biocompatibility, animal-free origin and mechanical stability. Here, we investigated BNC as a vehicle for human embryonic stem cells-derived LSC (hESC-LSC). To enhance cell-biomaterial interactions, we implemented a plasma activation followed by a Collagen IV and Laminin coating of the BNC substrates. This surface functionalization with human extracellular matrix proteins greatly improved the attachment and survival of hESC-LSC without compromising the flexible, robust and semi-transparent nature of the BNC. The surface characteristics of the BNC substrates are described and a preliminary ex vivo test in simulated transplantation scenarios is provided. Importantly, we show that hESC-LSC retain their self-renewal and stemness characteristics up to 21 days on BNC substrates. These results open the door for future research on hESC-LSC/BNC constructs to treat severe ocular surface pathologies.

2. KEYWORDS

- Microbial cellulose
- Corneal epithelium
- Human embryonic stem cells
- Animal-free
- Cell transplantation

3. GRAPHICAL ABSTRACT



4. INTRODUCTION

Limbal stem cells (LSC) are tissue-specific stem cells located at the boundary between the cornea and the bulbar conjunctiva. LSC safeguard ocular surface health by constantly renewing the corneal epithelium and by preventing the opaque conjunctival cells to migrate into the transparent cornea. [1][2] Acute trauma, burns and inflammatory diseases can disrupt the delicate ocular surface homeostasis and cause opacification, vascularization and scarring of the cornea resulting in impaired vision. [3][4] LSC

transplantation holds enormous therapeutic potential for these incapacitating conditions [5][6] [7] but its implementation is conditioned to the availability of clinically-compliant donor LSC and the effectiveness of the cell delivery strategies. [8][9] As an alternative to autologous and allogenic primary cell sources, on-demand amounts of LSC can be attained through differentiation from human induced pluripotent (hiPSC) or human embryonic stem cells (hESC) independently from donor ocular tissues. Furthermore, recent protocols ensure the reproducible and well-defined differentiation of LSC offering safer venues for ocular surface reconstruction. [10]–[12]

Finding an optimal carrier for LSC transplantation to the ocular surface would give a firm push to the practical implementation of LSC-based therapies. Ideally, the carrier should be biocompatible and support cell viability while presenting adequate material properties (*e.g.* robustness, conformability, manageability). Human amniotic membrane (AM), the innermost layer of the placenta, is widely used in ophthalmological treatments [13][14] and it has been advocated as a well-suited substrate for LSC expansion and transplantation. [15][16] Nevertheless, concerns about the low availability and reproducibility of AM have prompted research on alternative biological substrates such as collagen and fibrin. [17][18][19] On this line, we have previously suggested the biopolymer bacterial nanocellulose (BNC) for ocular surface bandaging applications. [20] BNC is biosynthesized by non-pathogenic bacterial cultures in the form of an interlaced nanofibrillar structure with high architectonic parallelism to collagen matrices. This nanostructure endows BNC with outstanding material properties regarding mechanical and thermal stability, conformability, water retention and easiness of manipulation. [21] In addition, BNC is widely regarded as a cytocompatible substrate owing to its high chemical purity and supported by numerous *in vitro* investigations [22] [23] [24]. As for immunogenicity, BNC grafts have been found to elicit low to none inflammatory responses *in vivo* and to be generally well tolerated by the surrounding tissues [25] [26] [27] [28]. Production-wise, BNC is equally appealing because of its animal-free origin, tunability and feasible scale-up. [29] [30] All these reasons endorse BNC towards its way through the health market [31][32] with applications ranging from wound dressings [33][34] to anti-fibrotic implant coatings. [35]

Here, we aimed at establishing and characterizing LSC cultures on BNC substrates to assess the potential of BNC as a transplantation vehicle for these cells. BNC has been suggested as a carrier for other cell types, [36][37] including retinal pigment epithelium, [38][39] but to the best of our knowledge, this is the first study combining BNC and LSC. Clinical translation being our ultimate goal; we employed LSC differentiated from hESC (hESC-LSC) under feeder- and serum-free conditions [11]. Similarly, BNC membranes were thoroughly purified until endotoxin-free before its use as cell support [22]. The palette of BNC modifications seeking to enhance cell attachment is particularly diverse [29] [30] [40] [41] [42]. Thus, our ambition was to find a BNC conditioning rendering a favourable interface for hESC-LSC culture in a simple, well-defined and scalable process.

5. MATERIALS AND METHODS

5.1. Bacterial nanocellulose (BNC) substrates preparation and characterization

5.1.1. BNC production

BNC hydrogels were synthesized by *Komagataeibacter xylinus* (*K. xylinus*, NCIMB 5346 from CECT, Valencia, Spain) grown on Hestrin-Schramm medium following our previously described protocols. [20][43] *K. xylinus* cultures were kept on 24-well plates for three days under static conditions at 30 °C to obtain circular BNC fleeces with the same diameter as the containers (~1.6 cm). The as-formed hydrogels were picked with tweezers and immersed in a 1:1 v/v solution of Milli-Q water and ethanol for 10-15 minutes. Then, BNC fleeces were cleaned with boiling Milli-Q water (40 min) and NaOH (2 x 20 min) to remove organic remains. The BNC hydrogels were dried at 60 °C, between two Teflon plates and 1 Kg weight. Dry films were rehydrated in Milli-Q water, sterilized by autoclave (121 °C, 20 min), and stored at room temperature until experimental use.

5.1.2. BNC surface modification

BNC membranes were placed on 24-well culture plates and incubated overnight at 4 °C with a solution of 0.5 µg/cm² of recombinant human laminin (LN-521, Biolamina) and 5 µg/cm² collagen type IV from human placenta (Col IV, Sigma-Aldrich) in Dulbecco's phosphate-buffered saline (DPBS, Lonza) containing calcium and magnesium. The as-prepared samples are referred to as “ECM coated” BNC.

To prepare the “Plasma + ECM coated” samples, dry BNC films were activated for 1 min with oxygen plasma inside a plasma reactor (Diener Electronic GmbH, power=50 W, pressure=0.40 mBar) under vacuum. Then, the activated membranes were immediately coated with the ECM protein solution following the previous procedure. The “plasma” BNC samples were only irradiated with oxygen plasma and the “plain” samples were left untreated.

5.1.3. Light transmittance measurements

Visible light absorption spectra were collected with a JASCO V-570 UV-Vis-NIR spectrophotometer between 400 and 800 nm. Samples were held with a cover glass also used for the baseline correction. Three different samples were analysed for each condition and the obtained values were averaged.

5.1.4. Scanning electron microscopy (SEM)

Fragments of dry BNC films were placed flat on aluminium SEM sample holders with adhesive carbon tape. Metalized samples were sputtered with 5 nm of platinum before imaging. A high-resolution scanning electron microscope (FEI Magellan 400L XHR SEM) was used under a high vacuum and with an acceleration voltage of 2 kV to obtain images at 5.000, 20.000 and 100.000X magnifications. Working distance was 4 mm and the current was 0.1 nA. Energy-dispersive X-ray (EDX) spectroscopy was performed with the same equipment at 1 KeV. At least two areas from four independent BNC samples were imaged on both sides of the films.

5.1.5. Atomic force microscopy (AFM)

Topographical images and roughness values were obtained with a 5100 Agilent Technologies atomic force microscopy on tapping mode and equipped with a FORT tip from AppNano. Three 30 x 30- μ m areas were analysed from each sample. Dry BNC samples were fixed flat on the holders with adhesive tape. The images were processed with Surface analysis software V7.4 (64-bit) - Mountains technology.

5.1.6. *Ex vivo* evaluation of BNC with porcine corneal organ culture

The corneal organ model employed in this study has been described previously [44] [45]. Briefly, fresh porcine eyes from a local abattoir were kept in cold DPBS + 2 % antibiotics for up to 4 h and then disinfected with 2 % povidone-iodine (Betadine®, Leiras). The corneas and part of the sclera were

resected under sterile conditions and kept in Dulbecco's Modified Eagle Medium (DMEM) supplemented with 5 % FBS, 1 % Penicillin/Streptomycin (P/S), 0.1 % Amphotericin-B and 1 X GlutaMax at 37 ° C and 5 % CO₂ until BNC implantation. Before the BNC application, epithelial damage was created by an exhaustive scraping of the corneal surface with a scalpel, including the limbal area. BNC membranes were preconditioned with culture medium and 5-mm diameter pieces were cut with a trephine and sutured to the central part of the cornea with the help of a Barron artificial anterior chamber (Katena products Inc.). Four symmetric sutures (VICRON suture number 7) were made to fix each BNC sample. Then, specimens were moved to 6-well plates and covered with soft contact lenses (EyeQ One-Day Premium, Cooper Vision) to avoid drying. The corneal organ culture was kept in the same culture conditions for two weeks after the implantation. The medium was changed twice per week. Before histological analysis, the porcine corneas were fixed using 4 % paraformaldehyde (PFA) in DPBS for 4 h at RT. Samples were dehydrated in a Tissue-Tek VIP 5 (Sakura Finetek Europe) automatic tissue processor overnight and embedded in paraffin blocks. Following, 7 mm thick tissue sections were cut with a microtome from each sample to cover different areas of the cornea. Histological sections were stained with haematoxylin-eosin (HE) and mounted on TOMO® adhesion microscope slides (Matsunami Glass Ind., Ltd.). Optical microscope images were captured with Nikon Eclipse TE2000-S microscope and DS-Fi1 camera.

5.2. In vitro experiments

5.2.1. Human embryonic stem cell-derived limbal stem cells (hESC-LSC) culture

All cell studies were conducted under the ethical approval of the Ethics Committee of Pirkanmaa Hospital District number R05116 to derive, culture and differentiate hESC lines for research. No new cell lines were derived from this study. The hESC-LSCs were differentiated from the hESC line Regea08/17 as described previously. [11] The hESC-LSC cultures were maintained under serum- and feeder cell-free conditions. For the *in vitro* experiments, cryopreserved hESC-LSC in PSC cryopreservation medium (Thermo Fisher Scientific) were thawed at 37 °C and directly plated on top of BNC substrates (100.000 cells/ cm²) placed on 24-well plates. Immediately after seeding, the culture plates were centrifuged for one minute at 200 g's to increase the contact between hESC-LSC and the

BNC supports. Controls were seeded on Corning® CellBIND 24-well plates with the same ECM coating ($5 \mu\text{g}/\text{cm}^2$ Col-IV + $0.5 \mu\text{g}/\text{cm}^2$ LN-521). The cultures were maintained in defined CnT-30 corneal differentiation medium (CELLnTEC, Advanced Cell Systems) containing 0.5 % antibiotics (P/S) at 37 °C and 5 % CO₂. Cell morphology and attachment were visually evaluated with a phase-contrast microscopy Zeiss Axio Vert A1 (Carl Zeiss) and the medium was changed trice per week.

5.2.2. Cell viability studies

For qualitative cell viability assessment, the LIVE/DEAD® Viability/Cytotoxicity Kit for mammalian cells from Thermo Fisher Scientific was employed following the manufacturer's instructions. Briefly, cell cultures were washed with DPBS and incubated in the dark for 30 min with 500 μL of a 2 μM Calcein-AM and 1 μM Ethidium homodimer solution in DPBS. Then, the samples were rinsed with DPBS and imaged using a fluorescence microscope (Olympus IX51 equipped with a DP71 camera) at 10X. The PrestoBlue™ cell viability reagent (Thermo Fischer Scientific) was used to measure cell proliferation. Triplicate samples were washed with DPBS and incubated with PrestoBlue® reagent diluted 1:10 (v/v) in CnT-30 medium for 30 min at 37 °C and protected from light. Then, the supernatants were pipetted in technical triplicates on a 96-well plate (100 μL /well) and fluorescence values were read with a Viktor 1420 Multilabel Counter (Wallac) at 544 nm excitation and 590 emission wavelengths. Blanks were made with BNC substrates without cells. The average viability values obtained at Days 3 and 7 were normalized to values from Day 1 and represented as mean \pm standard error repeating the experiment three times.

5.2.3. Immunofluorescence

For specific marker proteins and Collagen IV detection, samples were firstly washed with DPBS, fixed with 4 % PFA for 20 min at RT and washed again three times with DPBS. Triton X-100 was used to permeabilize the cell membranes for 15 min at RT and then samples were blocked for 90 min with a solution of 3 % BSA in DPBS under mild agitation. Primary antibodies were diluted in 0.5 % BSA and incubated overnight at 4 °C. The next day, specimens were washed three times with DPBS and incubated for one hour at RT under mild agitation with the fluorescently labelled secondary antibodies diluted in 0.5 % BSA. See Table 1 for information regarding the employed antibodies. Finally, samples were

rinsed again three times with DPBS, flipped upside down and prepared for imaging with mounting medium containing 4',6-Diamidino-2-phenylindole di-hydrochloride (DAPI) (Vectashield® from Vector Laboratories) under 13 mm Ø coverslips. Pictures were captured using an Olympus IX51 fluorescence microscope with 5X and 10X dry objectives. The stainings were repeated at least three times. Raw images were coloured and adjusted for contrast and brightness using Image-J-Fiji software. Grey values were measured as the average intensity from the whole fluorescent images acquired with the same exposure times using the same software.

Table 1: Antibodies employed in the immunofluorescence staining.

Antibody	Host	Supplier	Dilution (v/v)
p63α	Rabbit	Cell Signalling Technology	1:200
p40	Mouse	Biocare Medical	1:100
CK14	Mouse	R&D	1:200
CK15	Mouse	Neomarkers (Thermo Fisher)	1:200
CK12	Goat	Santa Cruz Biotechnology	1:200
CK12	Rabbit	Abcam	1:200
Ki-67	Rabbit	Millipore	1:500
Collagen IV	Goat	Millipore	1:100
anti-rabbit Alexa-488	Donkey	Molecular Probes	1:800
anti-rabbit Alexa-568	Donkey	Molecular Probes	1:800
anti-goat Alexa-568	Donkey	Molecular Probes	1:800
anti-mouse Alexa-647	Donkey	Molecular Probes	1:800
Anti-mouse-Alexa-568	Donkey	Molecular Probes	1:800

5.2.4. Confocal microscope

Fixed hESC-LSC cultures grown on top of BNC membranes were incubated for 5 min at RT with 1 mL of a solution of 5 µg/mL CellMask™ Deep Red Plasma Membrane Stain (Invitrogen) to dye cellular membranes and 0.25 mg/mL Fluorescent Brightener (Sigma) diluted in DPBS to stain the BNC

substrates. Then, samples were rinsed with DPBS and placed with the cells facing down on Ibidi Glass Bottom dishes. Stack images were obtained with a confocal laser-scanning microscope (Leica SP5). Fluorescent Brightener was excited at 350 nm and Cell Mask 588 nm wavelengths. Fluorescence images were reconstructed and coloured with the Fiji package of Image-J (64-bit version).

5.3. Statistical analysis

Statistically significant differences were determined using Graph Pad Prism 5 software by one-way analysis of variance (ANOVA) and Tukey's multiple comparison *post hoc* test. Significance between groups was established for $P < 0.05$. Values provided correspond to the average \pm standard deviation or standard error of the mean as indicated. P-values on the graphs are summarized as non-significant (ns) for $P \geq 0.05$, * for $P < 0.05$, ** for $P < 0.01$ and *** for $P < 0.001$.

6. RESULTS

6.1. BNC membranes coating and characterization

BNC membranes (*i.e.* dried and rehydrated native BNC hydrogels) were conditioned for hESC-LSC culture following the process summarized in Figure 1A. Typically, hESC-LSC require specific binding moieties present in the extracellular matrix (ECM) for adherence and survival. Therefore, a defined mixture of ECM proteins consisting of human Collagen IV (Col-IV) and recombinant human Laminin-521 (LN-521) was conjugated to endow BNC with specific linkers to favour cell attachment. Col-IV was fluorescently immunostained to investigate the distribution and abundance of the covering (Figure 1, B-E). The conventional method consisting of incubating the BNC membranes with the protein solution rendered an inhomogeneous and incomplete coating of the substrates (Figure 1C) with accumulations of Col-IV in the cavity-like structures of the BNC membranes. To address this issue, a plasma activation step was incorporated before the impregnation with Col-IV and LN-521. The plasma-treated BNC substrates were homogeneously and more profusely covered by Col-IV than the substrates coated without prior plasma activation (Figure 1D). This effect was confirmed by comparing the fluorescence intensity values (Figure 1E) which showed statistically significant differences between the two methods.

Macroscopically, BNC membranes were indistinguishable. All the studied forms of BNC appeared as semi-transparent, thin (~20 microns) flexible and self-standing substrates (Figure 2A). BNC membranes, regardless of the surface treatments, were easily manipulated with tweezers and showed good conformability to a dome-shaped surface (Figure 2A). Moreover, the applied surface treatments had a negligible effect on the light transmittance of the BNC membranes (Figure 2B). All the investigated BNC membranes presented high light transmittance at long wavelengths while showing a gradual decline towards smaller wavelengths. As an example, the average transmittance at 700 nm was 84 % and 70% at 500 nm.

SEM was used to investigate the effect of oxygen plasma on the micro/nanostructure of BNC revealing an altered nanofiber morphology after the plasma treatment (Figure 1, F and H). This is a superficial modification since the reverse side of all the substrates presented the typical BNC nanofibrous organization (see a representative image in Figure 1I). Under SEM, the ECM coating was visually imperceptible on both ECM-coated and plasma-activated + ECM-coated samples (Figure 1, G and H). To discard misinterpretations due to the metallization of the samples, non-metallized substrates were also observed under SEM with comparable outcomes (Figure S1). On the contrary, a nitrogen peak, ascribed to the proteinaceous coating, was detected by EDX only on the samples containing Col-IV and LN-521 (Figure S1). Besides, the surface of the plasma-treated BNC membranes was noticeably rougher than the untreated ones. This observation was confirmed by AFM roughness measurements, which disclosed a 1.4-fold increase in roughness for the plasma-activated samples *vs* the not activated samples (AFM images are shown in Figure S1).

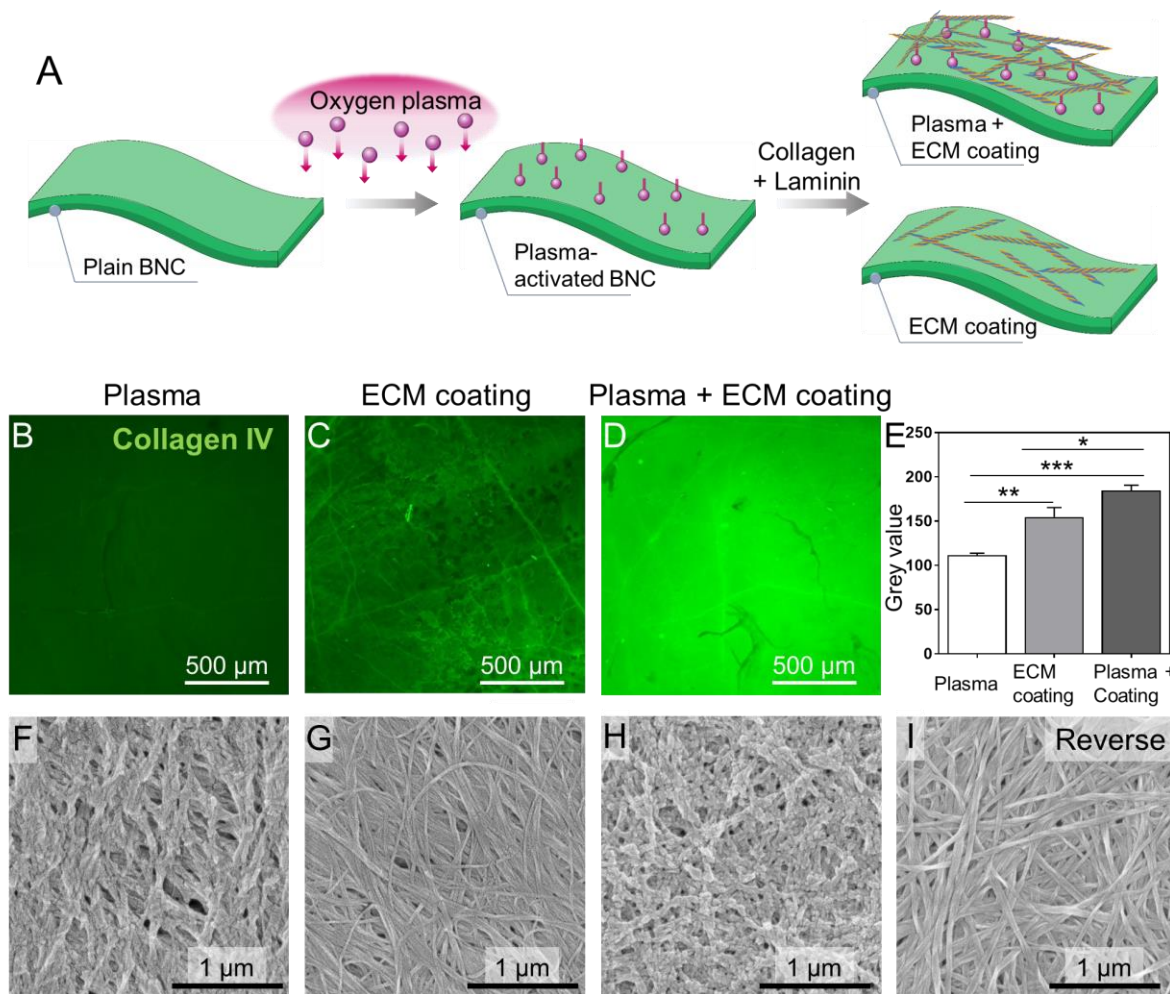


Figure 1: BNC surface treatments. A) Sketch of the different surface modifications of BNC membranes. B-D) Immunofluorescence staining of Collagen IV (green) deposited on BNC substrates. B) BNC activated with plasma but without ECM coating (Blank). C) BNC coated with the standard procedure consisting of pipetting the ECM protein solution on top of the substrates. D) Plasma-activated and ECM-coated BNC substrates where an intense and homogeneous coating by Collagen IV is observed. E) Fluorescence intensity (grey value \pm standard error) comparison of the Collagen IV staining between the different BNC substrates. Statistically significant differences were detected between all the groups. The lower board (F-I) gathers representative SEM images of the BNC substrates. As seen in images F and H, the plasma treatment altered the BNC nanofibers while the ECM coating was visually undetectable (G). I) The reverse (untreated) side of all the BNC substrates remained unaltered, indicating that the modifications caused by the oxygen plasma are superficial. A representative SEM image is shown.

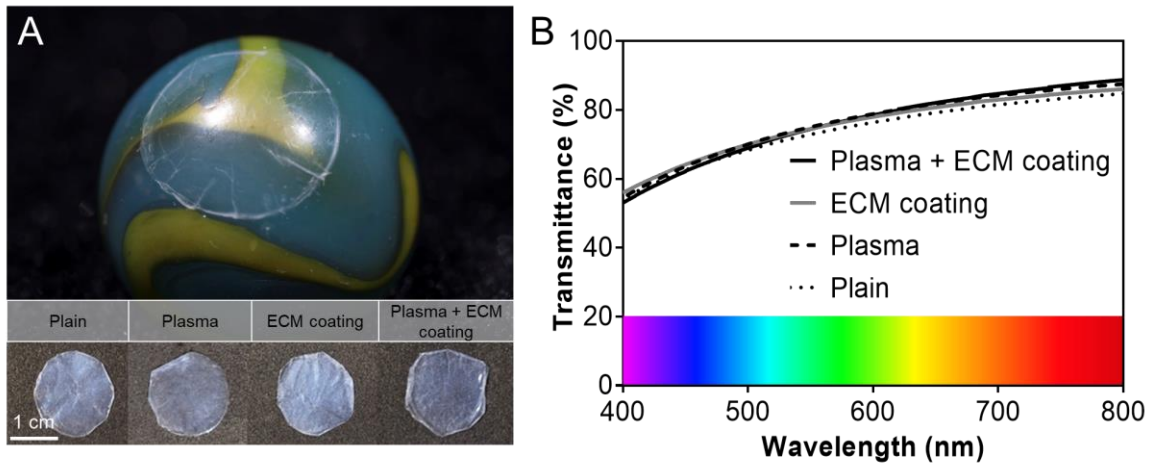


Figure 2: Macroscopic and optical features of BNC substrates. A) Digital images of the tested BNC substrates presenting an analogous appearance. All the membranes could be easily handled, maintained its flexibility and robustness and accommodated well to a curved surface (upper photograph). B) Visible light transmittance of the tested cell carriers. The coatings to enhance hESC-LSC attachment did not alter the optical properties of BNC. All the substrates presented high transmittance at long wavelengths with a progressive decrease towards shorter wavelengths.

6.2. *Ex vivo* BNC evaluation with a corneal organ culture

To assess the applicability of BNC as a support for cell transplantation to the ocular surface, an *ex vivo* organ culture model was used. Epithelial damage was created on excised porcine corneas before BNC implantation. After 14 days in culture, histological analysis was carried out by sectioning the specimens as schematized in Figure 3A. During the sample preparation process, BNC membranes proved excellent conformability to the dome shape of the corneas, could be cut to the desired size and were easily *ex vivo* sutured to the ocular surface (Figure 3B). Imaging of the HE-stained sections showed undamaged BNC membranes in close contact with the corneal surface for some of the tested eyes. Remarkably, a continuous corneal epithelium had re-grown under the BNC patch (Figure 3, C and D). See Figure S2 for comparison with a control pig cornea without BNC implantation where a similarly regrown pig epithelium is appreciable.

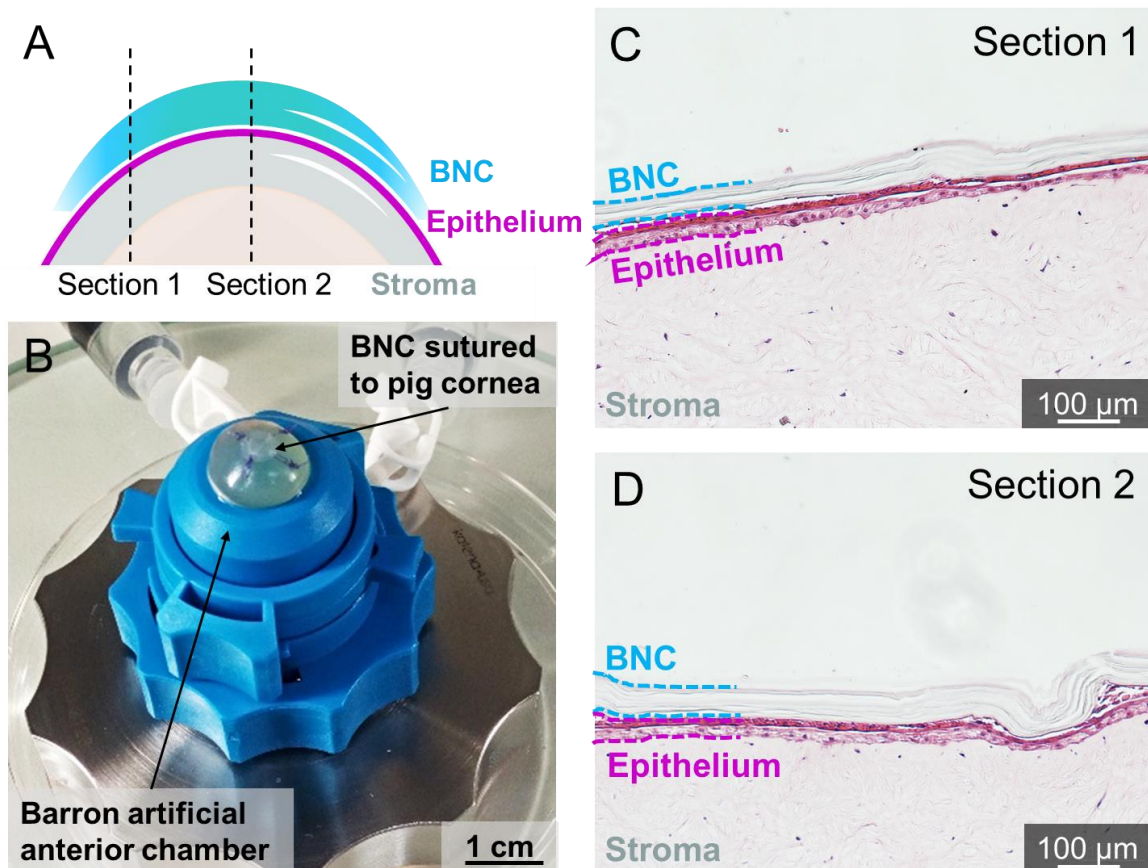


Figure 3: *Ex vivo* evaluation of BNC applicability as a cell delivery vehicle to the ocular surface with a porcine organ culture model. A) and B) depict the experimental setup, a Barron artificial anterior chamber (B) was used to perform the sutures on resected pig eyes. BNC membranes withstood cutting to the desired shape and fixation by suture stitches to porcine corneas with induced epithelial damage. Histological sections were cut as illustrated in A). HE staining of the tissue sections revealed the successful reepithelization of the pig corneas and intimate contact between the BNC and the ocular surface at the two examined areas (C and D). For clarity of the images, BNC has been highlighted in blue and the pig epithelium in pink.

6.3. hESC-LSC attachment and viability on BNC substrates

Next, the ability of the BNC to promote hESC-LSC attachment and viability was evaluated and compared for the distinct surface treatments. After 24 h in culture, evident differences could be observed in terms of cell morphology (Figure 4). hESC-LSC plated on plasma activated-ECM coated BNC membranes exhibited a homogeneous distribution on the substrate and the expected epithelial cell appearance (Figure 4D). Oppositely, hESC-LSC seeded on BNC membranes that received only plasma activation (Figure 4B) or solely ECM coating (Figure 4C) were round in morphology indicating poor

suitability of these substrates for hESC-LSC maintenance. The same outcomes were detected for plain BNC (Figure 4A).

In accordance with these observations, at Day 4 after seeding, Live/Dead staining evidenced a highly viable cell population on the BNC membranes that were plasma-activated and coated with Col IV and LN-521 (Figure 4H). hESC-LSC on plasma-activated as well as plain BNC had mainly detached from the substrates (Figure 4, E and F). On BNC membranes with conventional ECM coating, more hESC-LSC remained adhered but were unable to spread and stained mainly as dead cells (Figure 4G). An additional Live/Dead assay was conducted for BNC with plasma activation and ECM-coating at Day 8 to confirm long-term cell survival observing a highly viable hESC-LSC population (Figure S3). In light of these results, the *in vitro* experiments that follow were only performed with BNC substrates with plasma activation and ECM coating and are referred to as “BNC” from here on.

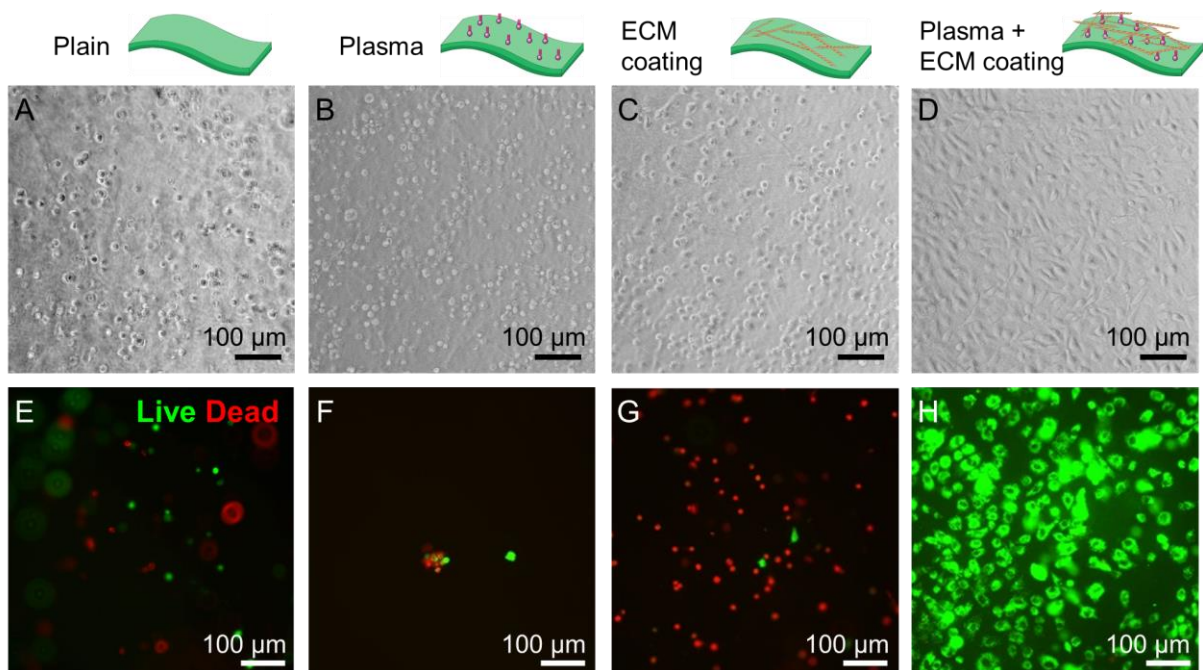


Figure 4: Attachment and viability of hESC-LSC on surface-modified BNC. A-D) Phase-contrast microscope images a Day 1 where, depending on the surface modification of BNC, clear differences in cell morphology can be visualized. Substrates with only one treatment (plasma (B) or ECM coating (C)) rendered rounded hESC-LSC morphologies while the combination of both created a favourable surface for hESC-LSC spreading (D). E-H) Live/Dead staining of hESC-LSC at Day 4 where alive cells are stained in green and dead cells in red. Note the

high cell viability in H corresponding to BNC substrates with plasma activation followed by ECM protein coating. Viable hESC-LSC on the rest of the substrates were scarce (E-G).

6.4. hESC-LSC self-renewing capacity on BNC substrates

Since the capacity to promote cell attachment, proliferation and then further differentiation towards corneal epithelial cells is a valuable characteristic of a cell carrier, we studied the self-renewal properties of hESC-LSC on BNC substrates at three different time points. Visually, an increase in cell number could be observed between Day 1 and 3 while from Day 3 to 7 cell density stabilized and cell size augmented (Figure 5A). hESC-LSC exhibited the expected cobblestone morphology at the three studied time points and tended to form an epithelial monolayer on top of the BNC substrates as observed by confocal microscope (Figure 5B). The metabolic activity was quantitatively analysed with a Presto Blue assay (Figure 5D). An increase in the fluorescence signal was detected at the early stages of the culture but not at the late stages where the fluorescence intensity remained constant (not statistically significant differences). To further confirm these results, immunofluorescence staining of the proliferation marker Ki67 was performed (Figure 5C). Expression of Ki67 was detected at Days 1, 3 and 7 in a fraction of the hESC-LSC indicating the presence of a self-renewing cell population. The estimated percentage of Ki67 positive cells was higher on Day 1 than on Day 7. hESC-LSC growing on conventional culture plates coated with Col IV and LN-521 were used for comparison and a similar evolution was observed (See Figure S4).

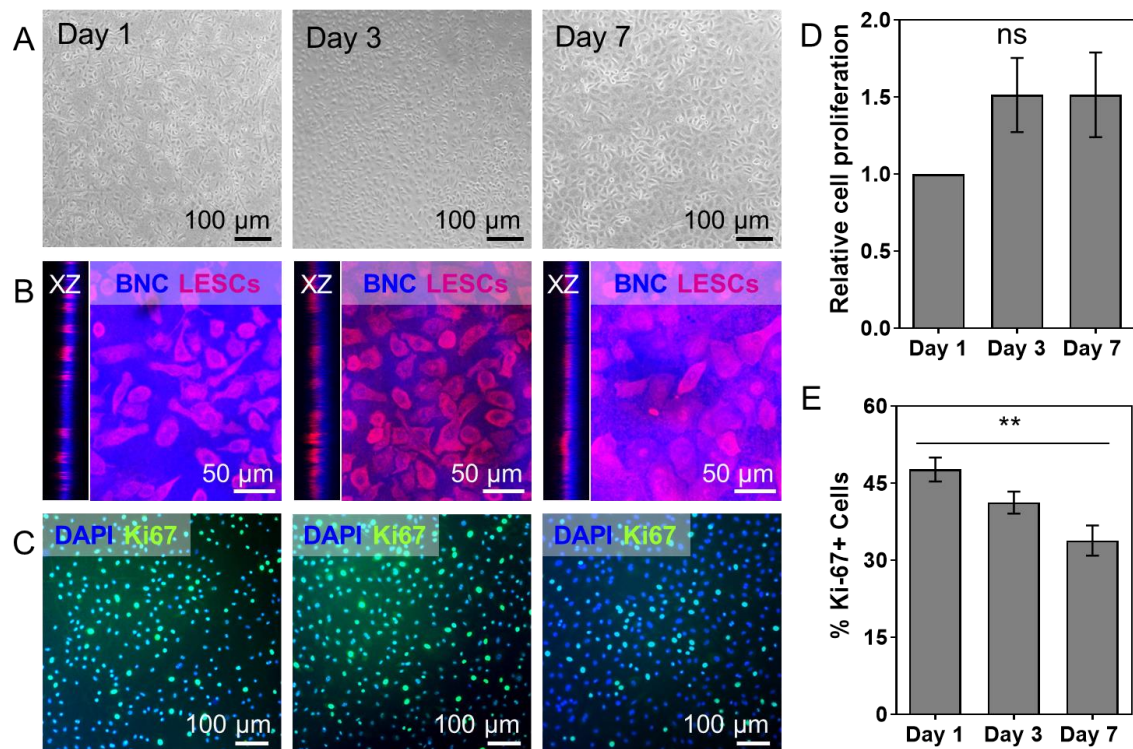


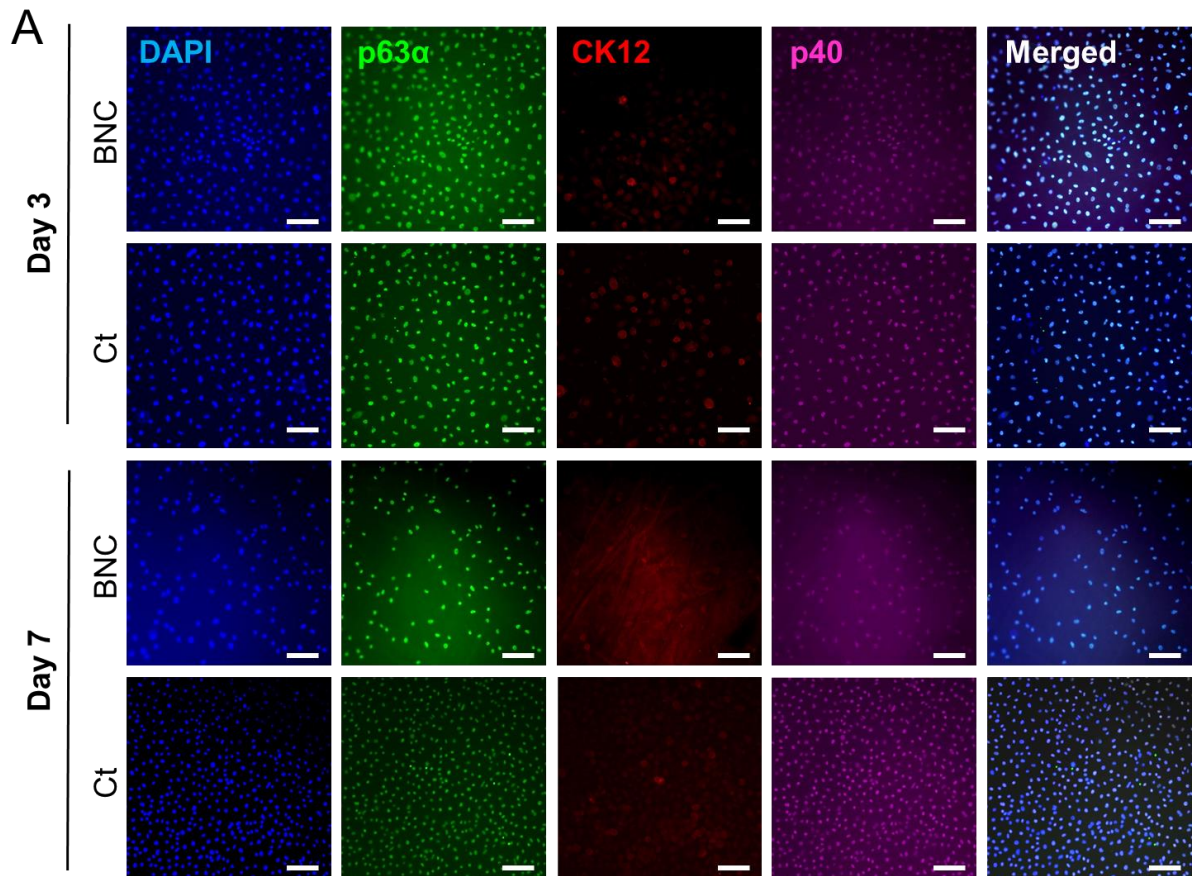
Figure 5: hESC-LSC culture monitoring and proliferation on BNC supports. A) Cell density and distribution vs. time on BNC substrates. B) Confocal microscope and XZ cross-section images where the tendency of hESC-LSC to form an epithelial monolayer on top of the BNC substrates can be observed. hESC-LSC plasma membranes were marked in red and the BNC supports in blue. C) Representative immunofluorescence staining images of the Ki67 proliferation marker expression at diverse time points of hESC-LSC cultures on BNC. D) Presto Blue assay measuring the metabolic activity of hESC-LSC expanded on BNC. Bars show the average value of three independent experiments with SEM. E) Estimation (average and SEM) of the percentage of Ki67-positive cells at three different culture time points.

6.5. Protein marker expression

Finally, we investigated whether hESC-LSC cultured on BNC films retain their progenitor phenotype or they start to differentiate towards corneal epithelial cells. The expression of specific LSC markers [46] was evaluated by immunocytochemistry. Simultaneous p63 α and p40 antibodies were used to detect the presence of the Δ Np63 α isoform of p63 in the cell nuclei, a widely used LSC marker. For further validation of the progenitor phenotype, the presence of distinctive cytokeratins (CK) was also examined. CK14 and CK15 were selected as stemness indicators while CK12 was employed as a

differentiated corneal cell marker. Immunofluorescence images shown in Figure 6A illustrate that the majority of hESC-LSC cultured on BNC substrates highly express $\Delta Np63\alpha$ and low to undetectable levels of CK12 at both Days 3 and 7 correlating with the expected LSC phenotype. Control hESC-LSC cultured on ECM-coated plastic exhibited a comparable marker expression pattern (see Ct in Figure 6A). Notably, the progenitor markers CK14 and CK15 behaved differently. While both keratins presented positive immunofluorescence –less homogeneous than $\Delta Np63\alpha$ – at Day 4, only CK15 remained detectable on hESC-LSC maintained on BNC membranes until Day 7 (Figure 6B). As for controls, a similar trend was observed except for some faint signal still present at Day 7 for CK14.

Furthermore, we examined the long-term maintenance of stemness marker expression. Figure S5 displays immunofluorescence micrographs of hESC-LCS on BNC carriers and control surfaces cultured for 2 and 3 weeks where a sustained LSC phenotype (p40-positive and predominantly CK12 negative) is perceived for both time points and culture surfaces resembling the early time points.



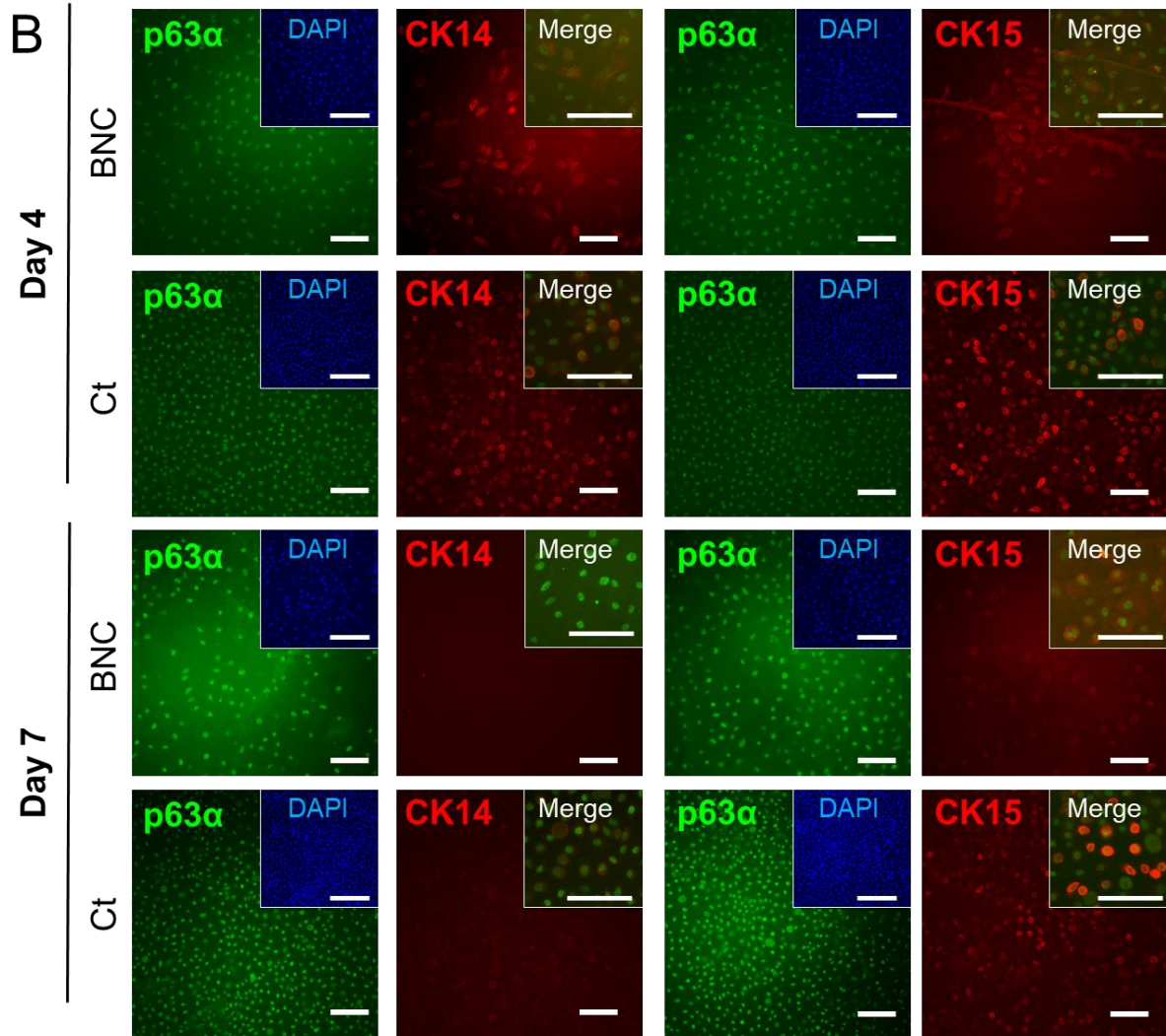


Figure 6: LSC marker expression at early time points. A) Representative immunofluorescence photographs of hESC-LSC cultured on BNC membranes 3 and 7 days after plating. Expression of the well-established limbal stem cell marker $\Delta Np63\alpha$ was confirmed by the simultaneous detection of p63 α and p40. CK12, an epithelial differentiation marker, was identified in low amounts. Merged images confirm the nuclear location of $\Delta Np63\alpha$ and the co-localization of the p63 α and p40 antibodies. Ct refers to conventional ECM-coated cell culture surfaces used for comparison and the scale bar is 100 μm . B) Cytoplasmic expression of the stemness-associated cytokeratins 14 and 15 (CK14 and CK15) on hESC-LSC cultures grown on top of BNC membranes for 4 and 7 days. The distribution of CK14 and CK15 (red) is compared to p63 α (green) present in the nucleus. Scale bar equals to 100 μm . Inserts: DAPI-stained nuclei (blue) to evidence the total number of cells and details of the localization of the stemness markers. Scale bar of the inserts= 50 μm .

7. DISCUSSION

hESC-LSC could revolutionize the management of ocular surface diseases but an optimal cell delivery strategy still needs to be found. This study suggests BNC as a non-animal sourced substrate for hESC-LSC maintenance, manipulation and plausible transplantation. We describe a straightforward plasma-assisted method to anchor ECM proteins on the surface of BNC enabling subsequent hESC-LSC attachment, spreading and viability. Then, we demonstrate that hESC-LSC cultures express the proliferation marker Ki67, especially at the early stages of the culture, and that they retain a limbal stem cell phenotype for up to 3 weeks on BNC supports.

A preliminary histological analysis from a corneal organ culture model shows the possibility to achieve intimate contact between BNC and the corneal surface, which is an advantageous situation for cell transplantation. We also observed re-epithelization under the BNC membranes, which hints that BNC does not cause major cytotoxicity or oxygen permeability issues on this *ex vivo* model. These findings, combined with our previous reports on BNC suturability and stability in contact with ocular tissue, [20] confirm that the material properties of BNC are adequate for a carrier in ocular surface cell replacement therapies. However, future research is required to assess the migration and integration capabilities of hESC-LSC grown on BNC carriers onto damaged corneas. Likewise, *in vivo* biocompatibility studies about ophthalmological applications of BNC are encouraging but still very scarce [47] and the interactions between BNC and the host ocular immune system warrant further investigation.

There are a few examples in the literature about the usage of BNC supports in stem cell culture that do not report on the need for coating BNC with ECM proteins to provide cell adhesion moieties. [48]–[50] Similarly, in our previous work with human dermal fibroblasts, [22] we found that BNC coating was not required to facilitate cell attachment. However, the here presented results prove that the plasma-assisted ECM protein functionalization is crucial for hESC-LSC attachment and survival on the BNC substrates. Neither the plasma activation alone nor the conventional method to coat cell culture surfaces were able to provide a favourable interface between BNC and hESC-LSC. These observations discard that the described enhanced hESC-LSC adhesion is a consequence of the increased roughness of the plasma-treated BNC substrates detected by electronic microscopy and AFM. On the contrary –and

backed by the intensified Col IV adsorption on plasma-treated BNC– we ascribe this effect on the presence of specific binding sites for hESC-LSC. Interestingly, an analogous strategy was followed by Sorkio *et al.* to enhance hESC-derived retinal pigment epithelial cells attachment to synthetic electrospun membranes drawing similar conclusions. [51] Hence, the requirement of surface modifications to use BNC as a cell culture substrate seems to be cell type-dependent. This cell-specificity has also been described by Pertile and colleagues[52] who reported that nitrogen plasma activation improved the affinity of microvascular cells and neuroblasts for BNC but had no effect on fibroblasts.

Notably, the plasma treatment (1 min-activation) did not make the hESC-LSC seeding protocol substantially longer, more complex or costlier compared to the standard ECM coating and did not compromise the manageability and the semi-transparency of the BNC membranes. By SEM examination, we encountered morphological changes on the BNC surface which were not present on the bulk of the material again in good agreement with reference. [52] Therefore, we conclude that plasma activation offers vast possibilities for BNC functionalization aiming at favouring its interactions with cells without comprising its outstanding materials properties in a fast, simple and scalable manner. [53]

We inferred hESC-LSC cultures progression on BNC by measuring the metabolic activity and by detecting the proliferation marker Ki67 noticing that hESC-LSC can produce new daughter cells on BNC membranes as evidenced by the presence of Ki67-positive populations. A slowdown on the proliferation rate after Day 3 together with an increase in cell size was detected. These features correlate with a slight maturation of the hESC-LSC on BNC, although not complete differentiation since the cultures remained positive for the LSC markers and essentially CK12 negative (maturation marker) for up to 3 weeks. The detection of the progenitor marker CK14 at Day 4 but not at Day 7 after plating and the dimmer staining for CK15 at Day 7 compared to Day 4 further supports that a partial maturation of hESC-LSC is occurring on the BNC carriers. We believe that is an interesting finding since cellular therapies expect the progeny of the transplanted cells to mature and become part of a functional corneal epithelium after implantation, mimicking the *in vivo* phenomena. [2][54]. On the other hand, the

employed hESC-LSC were previously proved capable of terminal differentiation on porcine collagen matrices by detecting the expression of CK3 and CK12 proteins. [19] However, it remains uncertain if hESC-LSC possess the ability to differentiate towards fully mature corneal epithelial cells on BNC supports indicating a need for future work. Together, these observations lead us to believe that the level of maturation of the hESC-LSC cultures will be an important parameter to consider in upcoming studies on BNC-assisted hESC-LSC delivery to the ocular surface.

Notably, the assumed long-term mode of action of LSC transplantation relies on its capability to repopulate the limbal niche and from there provide constant cell renewal to the corneal epithelium. The expression of multiple stemness markers – Δ Np63 α , CK14 and CK15– on hESC-LSC seeded on BNC carriers corroborates its progenitor phenotype and reinforces the therapeutic expectation that hESC-LSC could act similarly to autologous LSC [55][56]. Therefore, we venture that the time window between Day 1 and Day 4 after seeding on BNC supports could be an appropriate timing for hESC-LSC transplantation because the cultures exhibit higher proliferation and more stemness characteristics than later time-points; features that have been correlated with greater *in vivo* regenerative potential [57] [18]. Besides, this timing would also reduce the preparation period of the hESC-LSC/BNC constructs. Overall, and considering that biomaterial properties can greatly influence cell differentiation, [58][59] the ability of BNC membranes to maintain the hESC-LSC phenotype *in vitro* rather than inducing terminal differentiation is encouraging for future implementation. We speculate that this effect could be at least partially explained by the particular nanotopography of BNC, as already reported for mouse stem cell cultures. [48][60]

Currently, the library of biomaterials exploited in cell-based corneal regeneration is dominated by AM, [5][61] collagen [9][62] and fibrin-derived substrates [18][63] with successful results already reported. [18][64] Research efforts are now focused on reducing the inherent risks of these therapies [65] by switching to well-defined cell culture protocols [66][67] and non-animal sourced carriers. [68] In pursuit of clinically-compatible solutions, we employed serum- and feeder-free hESC-LSC cultures containing clinical-grade heparin, from the CnT-30 medium, as the only animal-derived product. BNC fits well into this emerging concept because of its purity and biotechnological animal-free production.

[69] We believe that BNC can be advantageous over the above-mentioned biopolymers because of its mechanical stability, manageability and lack of processing, which are considered as major limiting factors of the current solutions. [62][70] Moreover, the thermal stability of BNC enables both its sterilization by heat and cryopreservation. [22] The latest being of particular significance because it makes the cryobanking of ready-to-use hESC-LSC/BNC constructs a feasible possibility.

8. CONCLUSIONS

Here, we report on the culture of hESC-LSC on BNC membranes. We show that BNC substrates support the formation of new daughter cells and retain the progenitor phenotype of hESC-LSC while providing a self-standing and easy to manipulate mechanical support. Moreover, the non-animal origin of BNC and the well-defined hESC-LSC differentiation and cultivation procedures allowed the formation of cell-biomaterial constructs intended for a prospective clinical application in ocular surface treatments. hESC-LSC attachment and viability were achieved after a plasma-enabled ECM protein functionalization of the BNC substrates. This fast and simple BNC functionalization method could be exploited in the future for the culture of other therapeutic cells and expand the possibilities of BNC as a cell carrier.

9. ACKNOWLEDGEMENTS

This collaborative project was mainly funded with an EMBO short-term fellowship (ref 8288) awarded to IAS and the authors would like to express their gratitude to this institution. Researchers acknowledge financial support from the Spanish Ministry of Science and Innovation through the RTI2018-096273-B-I00 project, the *Severo Ochoa Programme* for Centres of Excellence in R&D (SEV-2015-0496 and CEX2019-000917-S) and the PhD scholarship of I.A.S. (BE-2017-076734) as well as Academy of Finland (326760). We are also grateful to Generalitat de Catalunya for the 2017SGR765 and the 2019LLAV00046 projects. Authors also appreciate Miquel Anton for his assistance with photography, the AFM service of ICMAB, the electron microscopy facility of ICN2 and the optical microscope service of UAB. The ICMAB members (I.A.S., A.L. and A.R.) participate in the CSIC Interdisciplinary Platform for Sustainable Plastics towards a Circular Economy, SUSPLAST, MICINN: “Research

Networks” nanoCARE, (RED2018-102469-T) and in the Aerogels COST ACTION (CA 18125). This work has been conducted within the Material Science Doctoral Program of the Autonomous University of Barcelona (I.A.S.).

Authors deeply thank the laboratory staff of Tampere University, especially Outi Melin and Hanna Pekkanen for the production, maintenance and differentiation of the hESCs and hESC-LSC, and Juha Heikkilä for the help with the plasma equipment. The authors acknowledge the Biocenter Finland (BF) and Tampere Imaging Facility (TIF) for their service.

10.CONFLICT OF INTEREST

The authors declare no conflicts of interest.

11.REFERENCES

- [1] A. V Ljubimov and M. Saghizadeh, “Progress in corneal wound healing,” *Prog Retin Eye Res*, vol. 49, pp. 17–45, 2015.
- [2] M. Ebrahimi, E. Taghi-Abadi, and H. Baharvand, “Limbal stem cells in review.,” *J. Ophthalmic Vis. Res.*, vol. 4, no. 1, pp. 40–58, Jan. 2009.
- [3] J. P. Whitcher, M. Srinivasan, and M. P. Upadhyay, “Corneal blindness: a global perspective. Bulletin of the World Health Organization,” 2001.
- [4] S. L. Wilson, A. J. El Haj, and Y. Yang, “Control of scar tissue formation in the cornea: strategies in clinical and corneal tissue engineering.,” *J. Funct. Biomater.*, vol. 3, no. 3, pp. 642–87, 2012.
- [5] N. Zakaria *et al.*, “Results of a phase I/II clinical trial: Standardized, non-xenogenic, cultivated limbal stem cell transplantation,” *J. Transl. Med.*, vol. 12, no. 1, p. 58, Mar. 2014.
- [6] J. Menzel-Severing, F. E. Kruse, and U. Schlötzer-Schrehardt, “Stem cell-based therapy for corneal epithelial reconstruction: present and future,” *Can. J. Ophthalmol.*, vol. 48, no. 1, pp. 13–21, 2013.
- [7] EuroStemCell, “Europe approves Holoclar®, the first stem cell-based medicinal product |

Eurostemcell.” [Online]. Available: <https://www.eurostemcell.org/story/europe-approves-holoclar-first-stem-cell-based-medicinal-product>. [Accessed: 27-Oct-2020].

[8] D. G. Harkin, S. E. Dunphy, A. M. A. Shadforth, R. A. Dawson, J. Walshe, and N. Zakaria, “Mounting of Biomaterials for Use in Ophthalmic Cell Therapies,” *Cell Transplant.*, vol. 26, no. 11, pp. 1717–1732, Nov. 2017.

[9] M. Ahearne, J. Fernández-Pérez, S. Masterton, P. W. Madden, and P. Bhattacharjee, “Designing Scaffolds for Corneal Regeneration,” *Adv. Funct. Mater.*, p. 1908996, Feb. 2020.

[10] H. Hongisto, M. Vattulainen, T. Ilmarinen, A. Mikhailova, and H. Skottman, “Efficient and scalable directed differentiation of clinically compatible corneal limbal epithelial stem cells from human pluripotent stem cells,” *J. Vis. Exp.*, vol. 140, p. e58279, 2018.

[11] H. Hongisto, T. Ilmarinen, M. Vattulainen, A. Mikhailova, and H. Skottman, “Xeno- and feeder-free differentiation of human pluripotent stem cells to two distinct ocular epithelial cell types using simple modifications of one method,” *Stem Cell Res. Ther.*, vol. 8, no. 1, p. 291, Dec. 2017.

[12] R. Hayashi *et al.*, “Generation of Corneal Epithelial Cells from Induced Pluripotent Stem Cells Derived from Human Dermal Fibroblast and Corneal Limbal Epithelium,” *PLoS One*, vol. 7, no. 9, p. e45435, Sep. 2012.

[13] A. Azuara-Blanco, C. T. Pillai, H. S. Dua, and D. H. Azuara-Blanco A, Pillai CT, “Amniotic membrane transplantation for ocular surface reconstruction,” *Br. J. Ophthalmol.*, vol. 83, no. 4, pp. 399–402, Apr. 1999.

[14] R. T. Pires, S. Tseng, and P. Prabbasawat, “Amniotic Membrane Transplantation for Bullous Keratopathy,” *Evidence-Based Eye Care*, vol. 1, no. 2, pp. 80–81, 2000.

[15] O. B. Selver *et al.*, “Corneal recovery in a rabbit limbal stem cell deficiency model by autologous grafts of tertiary outgrowths from cultivated limbal biopsy explants,” *Mol. Vis.*, vol. 22, pp. 138–149, Feb. 2016.

- 505 [16] S.-Y. Chen, M. Mahabole, and S. C. G. Tseng, "Optimization of Ex Vivo Expansion of Limbal
506 Epithelial Progenitors by Maintaining Native Niche Cells on Denuded Amniotic Membrane,"
507 *Transl. Vis. Sci. Technol.*, vol. 2, no. 7, p. 1, Nov. 2013.
- 508 [17] S. Mi, B. Chen, B. Wright, and C. J. Connon, "Ex vivo construction of an artificial ocular surface
509 by combination of corneal limbal epithelial cells and a compressed collagen scaffold containing
510 keratocytes," *Tissue Eng. - Part A*, vol. 16, no. 6, pp. 2091–2100, 2010.
- 511 [18] P. Rama, S. Matuska, G. Paganoni, A. Spinelli, M. De Luca, and G. Pellegrini, "Limbal stem-
512 cell therapy and long-term corneal regeneration," *N. Engl. J. Med.*, vol. 363, no. 2, pp. 147–155,
513 Jul. 2010.
- 514 [19] A. Mikhailova *et al.*, "Human pluripotent stem cell-derived limbal epithelial stem cells on
515 bioengineered matrices for corneal reconstruction," *Exp. Eye Res.*, vol. 146, pp. 26–34, May
516 2016.
- 517 [20] I. Anton-Sales *et al.*, "Bacterial nanocellulose as a corneal bandage material: A comparison with
518 amniotic membrane," *Biomater. Sci.*, vol. 8, no. 10, pp. 2921–2930, 2020.
- 519 [21] I. Anton-Sales, U. Beekmann, A. Laromaine, A. Roig, and D. Kralisch, "Opportunities of
520 Bacterial Cellulose to Treat Epithelial Tissues," *Curr. Drug Targets*, vol. 20, no. 8, pp. 808–
521 822, 2019.
- 522 [22] I. Anton-Sales, S. Roig-Sanchez, M. J. Sánchez-Guisado, A. Laromaine, and A. Roig, "Bacterial
523 nanocellulose and titania hybrids: cytocompatible and cryopreservable cell carriers," *ACS*
524 *Biomater. Sci. Eng.*, vol. 6, no. 9, pp. 4893–4902, Aug. 2020.
- 525 [23] L. Bacakova *et al.*, "Versatile Application of Nanocellulose: From Industry to Skin Tissue
526 Engineering and Wound Healing," *Nanomaterials*, vol. 9, no. 2, p. 164, Jan. 2019.
- 527 [24] L. Fu, J. Zhang, and G. Yang, "Present status and applications of bacterial cellulose-based
528 materials for skin tissue repair," *Carbohydr. Polym.*, vol. 92, no. 2, pp. 1432–1442, 2013.
- 529 [25] P. N. Mendes *et al.*, "In vivo and in vitro evaluation of an *Acetobacter xylinum* synthesized

530 microbial cellulose membrane intended for guided tissue repair.,” *Acta Vet. Scand.*, vol. 51, p.
531 12, 2009.

532 [26] I. F. Almeida *et al.*, “Bacterial cellulose membranes as drug delivery systems: An in vivo skin
533 compatibility study,” *Eur. J. Pharm. Biopharm.*, no. 3, pp. 332–336, 2013.

534 [27] S. Il Jeong, S. E. Lee, H. Yang, Y. H. Jin, C. S. Park, and Y. S. Park, “Toxicologic evaluation
535 of bacterial synthesized cellulose in endothelial cells and animals,” *Mol. Cell. Toxicol.*, vol. 6,
536 no. 4, pp. 373–380, 2010.

537 [28] G. Helenius, H. Bäckdahl, A. Bodin, U. Nannmark, P. Gatenholm, and B. Risberg, “In vivo
538 biocompatibility of bacterial cellulose,” *J. Biomed. Mater. Res. - Part A*, vol. 76, no. 2, pp. 431–
539 438, 2006.

540 [29] U. Beekmann *et al.*, “Process control and scale-up of modified bacterial cellulose production for
541 tailor-made anti-inflammatory drug delivery systems,” *Carbohydr. Polym.*, vol. 236, no.
542 December 2019, p. 116062, 2020.

543 [30] D. Kralisch, N. Hessler, D. Klemm, R. Erdmann, and W. Schmidt, “White biotechnology for
544 cellulose manufacturing--the HoLiR concept,” *Biotechnol Bioeng*, vol. 105, no. 4, pp. 740–747,
545 2010.

546 [31] D. Klemm *et al.*, “Nanocellulose as a natural source for groundbreaking applications in materials
547 science: Today’s state,” *Mater. Today*, vol. 21, no. 7, pp. 720–748, Apr. 2018.

548 [32] F. V. Ferreira *et al.*, “Porous nanocellulose gels and foams: Breakthrough status in the
549 development of scaffolds for tissue engineering,” *Mater. Today*, vol. 37, pp. 126–141, Apr.
550 2020.

551 [33] C.-N. Wu *et al.*, “TEMPO-Oxidized Bacterial Cellulose Pellicle with Silver Nanoparticles for
552 Wound Dressing,” *Biomacromolecules*, vol. 19, no. 2, pp. 544–554, Feb. 2018.

553 [34] S. Moritz *et al.*, “Active wound dressings based on bacterial nanocellulose as drug delivery
554 system for octenidine,” *Int. J. Pharm.*, vol. 471, no. 1–2, pp. 45–55, Aug. 2014.

- 555 [35] F. Robotti *et al.*, “Microengineered biosynthesized cellulose as anti-fibrotic in vivo protection
556 for cardiac implantable electronic devices,” *Biomaterials*, vol. 229, p. 119583, Jan. 2020.
- 557 [36] Y. K. Noh, A. Dos Santos Da Costa, Y. S. Park, P. Du, I. H. Kim, and K. Park, “Fabrication of
558 bacterial cellulose-collagen composite scaffolds and their osteogenic effect on human
559 mesenchymal stem cells,” *Carbohydr. Polym.*, vol. 219, no. February, pp. 210–218, Sep. 2019.
- 560 [37] C. Fey *et al.*, “Bacterial nanocellulose as novel carrier for intestinal epithelial cells in drug
561 delivery studies,” *Mater. Sci. Eng. C*, vol. 109, p. 110613, Apr. 2020.
- 562 [38] S. Gonçalves *et al.*, “Bacterial Cellulose As a Support for the Growth of Retinal Pigment
563 Epithelium,” *Biomacromolecules*, vol. 16, no. 4, pp. 1341–1351, 2015.
- 564 [39] S. Gonçalves *et al.*, “Acetylated bacterial cellulose coated with urinary bladder matrix as a
565 substrate for retinal pigment epithelium,” *Colloids Surfaces B Biointerfaces*, vol. 139, pp. 1–9,
566 Mar. 2016.
- 567 [40] S. Taokaew, M. Phisalaphong, and B.-M. Z. Newby, “Modification of Bacterial Cellulose with
568 Organosilanes to Improve Attachment and Spreading of Human Fibroblasts,” *Cellulose*, vol.
569 22, no. 4, pp. 2311–2324, Aug. 2015.
- 570 [41] F. K. Andrade, S. M. G. G. Moreira, L. Domingues, and F. M. P. P. Gama, “Improving the
571 affinity of fibroblasts for bacterial cellulose using carbohydrate-binding modules fused to
572 RGD,” *J. Biomed. Mater. Res. - Part A*, vol. 92, no. 1, pp. 9–17, Jan. 2010.
- 573 [42] R. Pértile, S. Moreira, F. Andrade, L. Domingues, and M. Gama, “Bacterial cellulose modified
574 using recombinant proteins to improve neuronal and mesenchymal cell adhesion,” *Biotechnol.*
575 *Prog.*, vol. 28, no. 2, pp. 526–532, 2012.
- 576 [43] S. Roig-Sanchez *et al.*, “Nanocellulose films with multiple functional nanoparticles in confined
577 spatial distribution,” *Nanoscale Horizons*, vol. 4, pp. 634–641, 2019.
- 578 [44] L. Koivusalo *et al.*, “Hydrazone crosslinked hyaluronan-based hydrogels for therapeutic
579 delivery of adipose stem cells to treat corneal defects,” *Mater. Sci. Eng. C*, vol. 85, no. 85, pp.

580 68–78, Apr. 2018.

581 [45] A. Sorkio *et al.*, “Human stem cell based corneal tissue mimicking structures using laser-assisted
582 3D bioprinting and functional bioinks,” *Biomaterials*, vol. 171, pp. 57–71, Jul. 2018.

583 [46] U. Schlötzer-Schrehardt and F. E. Kruse, “Identification and characterization of limbal stem
584 cells,” *Exp. Eye Res.*, vol. 81, no. 3, pp. 247–264, 2005.

585 [47] C. Zhang *et al.*, “Biocompatibility evaluation of bacterial cellulose as a scaffold material for
586 tissue-engineered corneal stroma,” *Cellulose*, vol. 27, no. 5, pp. 2775–2784, 2020.

587 [48] T. Tronser, A. Laromaine, A. Roig, and P. A. Levkin, “Bacterial Cellulose Promotes Long-Term
588 Stemness of mESC,” *ACS Appl. Mater. Interfaces*, vol. 10, no. 19, pp. 16260–16269, May 2018.

589 [49] M. Vielreicher, D. Kralisch, S. Völkl, F. Sternal, A. Arkudas, and O. Friedrich, “Bacterial
590 nanocellulose stimulates mesenchymal stem cell expansion and formation of stable collagen-I
591 networks as a novel biomaterial in tissue engineering,” *Sci. Rep.*, vol. 8, no. 1, p. 9401, Dec.
592 2018.

593 [50] A. Laromaine, T. Tronser, I. Pini, S. Parets, P. A. Levkin, and A. Roig, “Free-standing three-
594 dimensional hollow bacterial cellulose structures with controlled geometry *via* patterned
595 superhydrophobic–hydrophilic surfaces,” *Soft Matter*, vol. 14, no. 19, pp. 3955–3962, May
596 2018.

597 [51] K. Y. Li *et al.*, “Fish-Scale Collagen Membrane Seeded with Corneal Endothelial Cells as
598 Alternative Graft for Endothelial Keratoplasty Transplantation,” *ACS Biomater. Sci. Eng.*, vol.
599 6, p. 2570–2577, 2020.

600 [52] R. A. N. Pertile, F. K. Andrade, C. Alves, and M. Gama, “Surface modification of bacterial
601 cellulose by nitrogen-containing plasma for improved interaction with cells,” *Carbohydr.*
602 *Polym.*, vol. 82, no. 3, pp. 692–698, 2010.


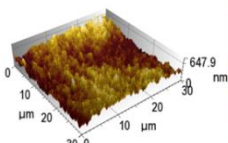
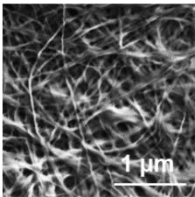
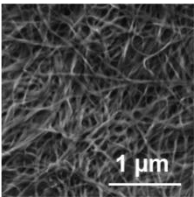
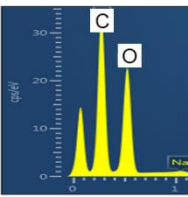
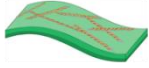
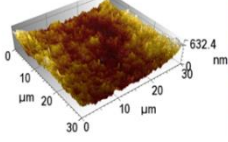
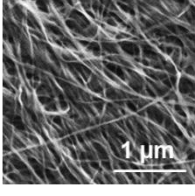
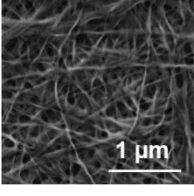
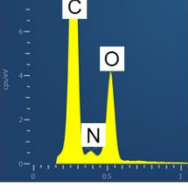
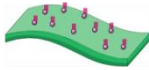
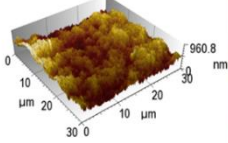
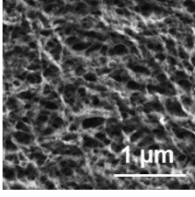
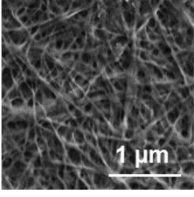
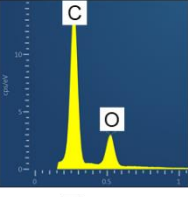
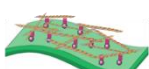
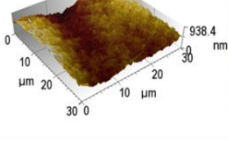
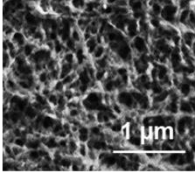
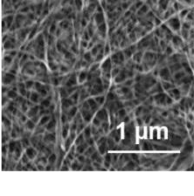
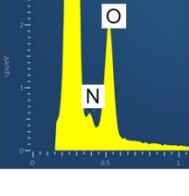
603 [53] N. Eswaramoorthy and D. R. McKenzie, “Plasma treatments of dressings for wound healing: a
604 review,” *Biophysical Reviews*, vol. 9, no. 6. Springer Verlag, pp. 895–917, 01-Dec-2017.

- 605 [54] J. J. Yoon, "Limbal stem cells: Central concepts of corneal epithelial homeostasis," *World J.*
606 *Stem Cells*, vol. 6, no. 4, p. 391, 2014.
- 607 [55] G. Pellegrini, C. E. Traverso, A. T. Franzi, M. Zingirian, R. Cancedda, and M. De Luca, "Long-
608 term restoration of damaged corneal surfaces with autologous cultivated corneal epithelium,"
609 *Lancet*, vol. 349, no. 9057, pp. 990–993, 1997.
- 610 [56] G. Pellegrini *et al.*, "Biological parameters determining the clinical outcome of autologous
611 cultures of limbal stem cells," *Regen. Med.*, vol. 8, no. 5, pp. 553–567, 2013.
- 612 [57] I. Massie, H. J. Levis, and J. T. Daniels, "Response of human limbal epithelial cells to wounding
613 on 3D RAFT tissue equivalents: Effect of airlifting and human limbal fibroblasts," *Exp. Eye*
614 *Res.*, vol. 127, pp. 196–205, 2014.
- 615 [58] N. Mitrousis, A. Fokina, and M. S. Shoichet, "Biomaterials for cell transplantation," *Nat. Rev.*
616 *Mater.*, vol. 3, pp. 441–456, Oct. 2018.
- 617 [59] S. Masterton and M. Ahearne, "Mechanobiology of the corneal epithelium," *Experimental Eye*
618 *Research*, vol. 177. Academic Press, pp. 122–129, 01-Dec-2018.
- 619 [60] N. Geisel *et al.*, "Microstructured Multilevel Bacterial Cellulose Allows the Guided Growth of
620 Neural Stem Cells," *Small*, vol. 12, no. 39, pp. 5407–5413, 2016.
- 621 [61] E. Y. X. Loh, N. Mohamad, M. B. Fauzi, M. H. Ng, S. F. Ng, and M. C. I. Mohd Amin,
622 "Development of a bacterial cellulose-based hydrogel cell carrier containing keratinocytes and
623 fibroblasts for full-thickness wound healing," *Sci. Rep.*, vol. 8, no. 1, p. 2875, Dec. 2018.
- 624 [62] S. Matthyssen, B. Van den Bogerd, S. N. Dhubhghaill, C. Koppen, and N. Zakaria, "Corneal
625 regeneration: A review of stromal replacements," *Acta Biomater.*, vol. 69, pp. 31–41, Mar. 2018.
- 626 [63] P. Rama *et al.*, "Autologous fibrin-cultured limbal stem cells permanently restore the corneal
627 surface of patients with total limbal stem cell deficiency," *Transplantation*, vol. 72, no. 9, pp.
628 1478–1485, Nov. 2001.

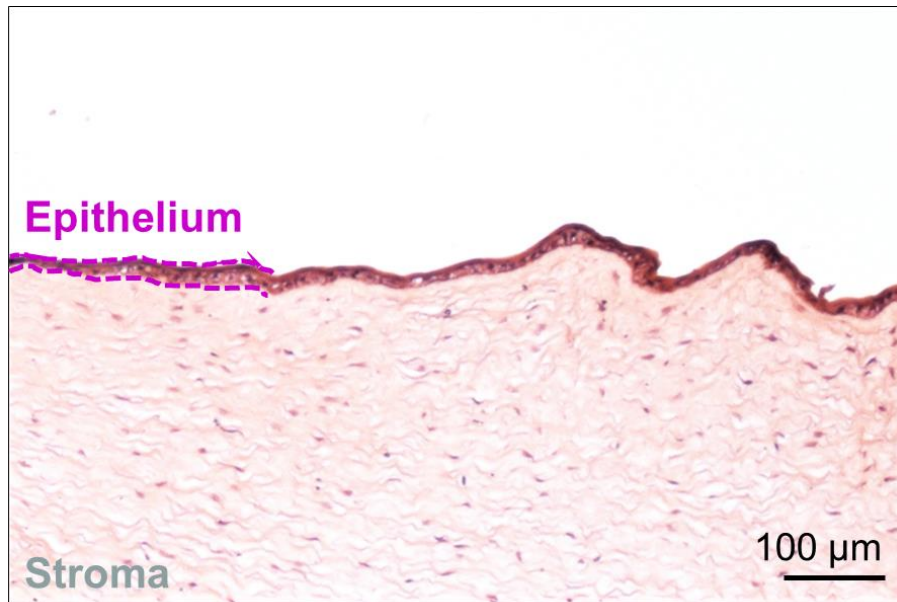
- [64] P. Fagerholm *et al.*, “Stable corneal regeneration four years after implantation of a cell-free recombinant human collagen scaffold,” *Biomaterials*, vol. 35, no. 8, pp. 2420–2427, Mar. 2014.
- [65] I. R. Schwab, N. T. Johnson, and D. G. Harkin, “Inherent risks associated with manufacture of bioengineered ocular surface tissue,” *Archives of Ophthalmology*, vol. 124, no. 12. American Medical Association, pp. 1734–1740, 01-Dec-2006.
- [66] N. Nieto-Nicolau, E. M. Martínez-Conesa, A. M. Velasco-García, C. Aloy-Reverté, A. Vilarrodona, and R. P. Casaroli-Marano, “Xenofree generation of limbal stem cells for ocular surface advanced cell therapy,” *Stem Cell Res. Ther.*, vol. 10, no. 1, p. 374, Dec. 2019.
- [67] T. Nakamura *et al.*, “The use of autologous serum in the development of corneal and oral epithelial equivalents in patients with Stevens-Johnson syndrome,” *Investig. Ophthalmol. Vis. Sci.*, vol. 47, no. 3, pp. 909–916, Mar. 2006.
- [68] L. Koivusalo *et al.*, “Tissue adhesive hyaluronic acid hydrogels for sutureless stem cell delivery and regeneration of corneal epithelium and stroma,” *Biomaterials*, vol. 225, no. September, p. 119516, Dec. 2019.
- [69] M. Cimino, R. M. Gonçalves, C. C. Barrias, and M. C. L. Martins, “Xeno-Free Strategies for Safe Human Mesenchymal Stem/Stromal Cell Expansion: Supplements and Coatings,” *Stem Cells Int.*, vol. 2017, p. 6597815, 2017.
- [70] Z. Chen *et al.*, “Biomaterials for corneal bioengineering,” *Biomed. Mater.*, vol. 13, p. 032002, 2018.

12.SUPPORTING INFORMATION

Figure S1: Substrate characterization. Table gathering information about surface characterization of BNC membranes undertaking different treatments. Column one shows atomic force microscopy (AFM) topographical pictures and average roughness values \pm standard deviation from three different 30 x 30- μ m images. Column two and three show scanning electron microscopy (SEM) micrographs of non-metallized BNC samples from both sides of the substrates (treated vs untreated). The fourth column shows EDX graphs from the same substrates. Note that a nitrogen peak is only detected on samples with ECM proteins coating.

BNC Substrate / characterization	AFM	SEM treated side	SEM untreated side	EDX
Plain 	Roughness= 83 ± 20 nm 			
ECM coating 	Roughness= 69 ± 21 nm 			
Plasma 	Roughness= 109 ± 11 nm 			
Plasma + ECM coating 	Roughness= 109 ± 37 nm 			

661 **Figure S2: Control pig cornea after epithelial damage.** HE-stained tissue section from a cultured
662 porcine cornea one week after inducing epithelial damage and without implanting BNC. The regrown
663 pig epithelium has been highlighted in pink.



664

Figure S3: hESC-LSC viability on Day 8. Fluorescent Live/Dead staining of hESC-LSC cultures on control surfaces (ECM-coated commercial culture plate) and BNC coated with ECM proteins after plasma activation. Viable cells are stained green with Calcein-AM and dead cells in red with Propidium Iodide. The right image demonstrates that hESC-LSC keep high viability on BNC supports after 8 days of culture.

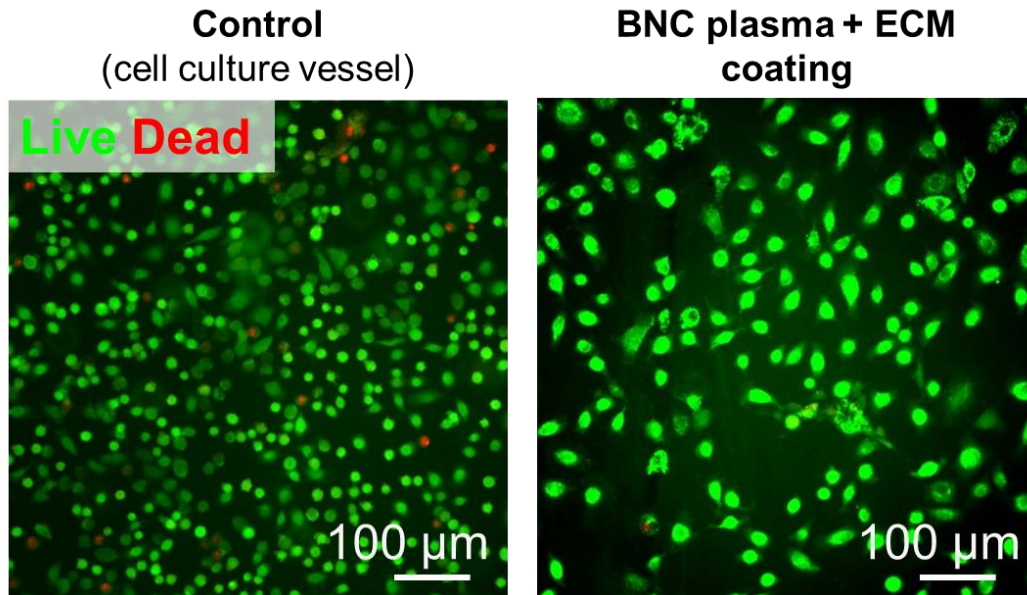


Figure S4: Monitoring of hESC-LSC cultures on control surfaces (ECM-coated cell culture plates). A) Phase-contrast microscope images at different time points. B) Immunofluorescence staining of the proliferation marker Ki67 (green). Cell nuclei are marked in blue (DAPI) to evidence the total number of cells.

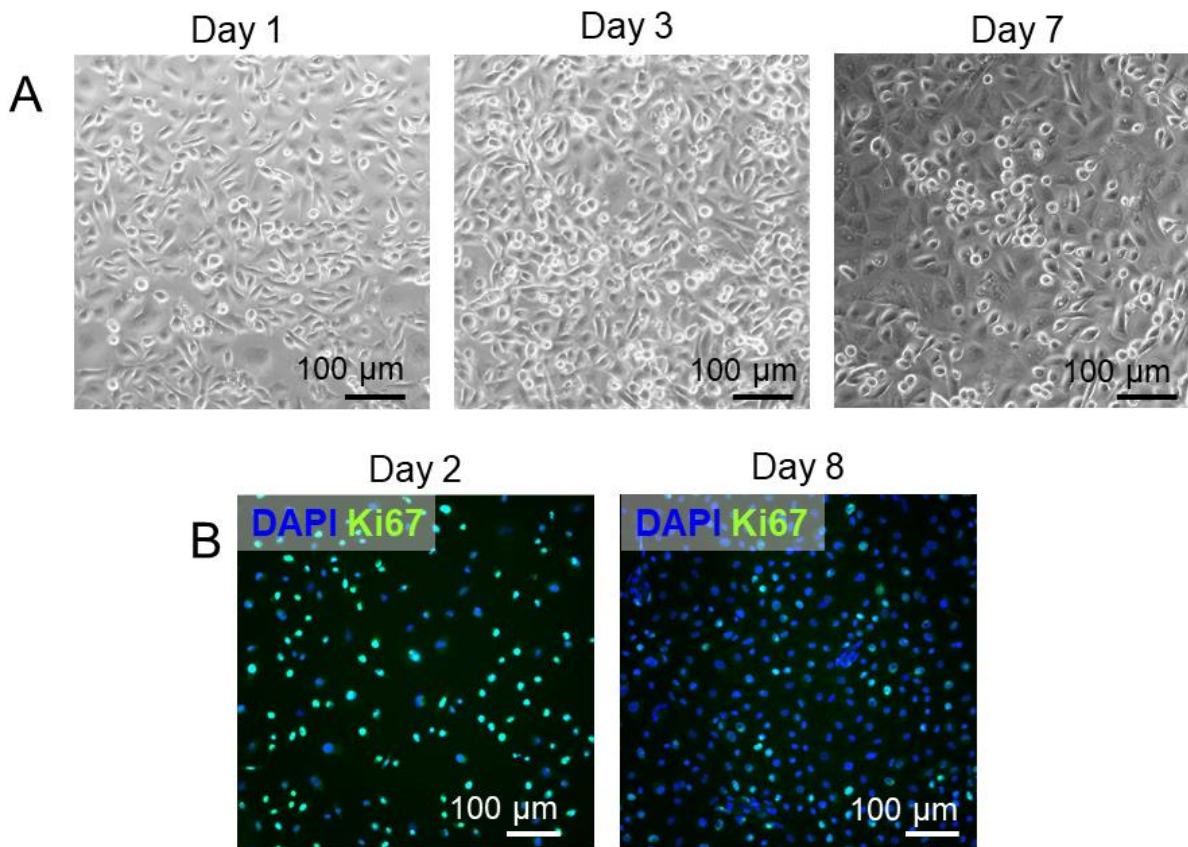


Figure S5: Protein marker expression profile of hESC-LSC after long-term culture. Characteristic immunofluorescence images of hESC-LSC maintained for two and three weeks on plasma-treated + ECM-coated BNC substrates and control surfaces (ECM-coated culture vessels). For all the pictures DAPI marks cell nuclei to show the total cell number, p40-positive cells are considered to exhibit a stemness phenotype and the dim CK12 (corneal maturation marker) signal indicates a predominantly low maturation stage of the cultures on both conditions and time points. Scale bar = 100 μ m.

